Talanta 82 (2010) 409–416

Contents lists available at ScienceDirect

Talanta

journal homepage: www.elsevier.com/locate/talanta

Short communication

Novel facile detection of persistent organic pollutants using highly sensitive gas sensor

Jinyun Liu[a], Fanli Meng[a], Tao Luo[a], Wei Li[b], Minqiang Li[a], Jinhuai Liu[a,*]

[a] The Key Laboratory of Biomimetic Sensing and Advanced Robot Technology, Institute of Intelligent Machines, Chinese Academy of Sciences, Hefei 230031, PR China
[b] Department of Automation, University of Science and Technology of China, Hefei 230026, PR China

ARTICLE INFO

Article history:
Received 6 January 2010
Received in revised form 2 April 2010
Accepted 6 April 2010
Available online 13 April 2010

Keywords:
Nanostructure
Environmental monitoring
Gas sensor
Sensitivity

ABSTRACT

Persistent organic pollutants (POPs) are greatly noxious chemicals in environment, and they can cumulate in organisms and transfer between different species. Therefore, it is significant to detect POPs for both environmental evaluation and further treatment. However, developing facile approach for the detection of POPs still remains a challenge so far. In this paper, we report an innovative method for facile detection of POPs using gas sensor for the first time. Porous SnO_2 nanostructures with a special tri-walled structure prepared via hydrothermal route and annealing process, were employed as gas-sensing materials. Through gas measurements, it was revealed that the as-fabricated gas sensor exhibited highly sensitive performance towards target POPs, including methoxychlor, mirex, p,p′-DDT, and aldrin. Moreover, we found that target POPs were distinguishable by extracting characteristics in kinetic curves of gas adsorption–desorption. As the presented detecting approach is facile without the requirements of complex operations, expensive and bulky instruments, it is expected that it would be developed as a promising method for the detection of POPs, and thereby showing its significance for environmental monitoring.

1. Introduction

Environmental issue has received increasing attention due to its great impact on all creatures on the earth. In the past decades, various pollutants have been released from industrial manufacture, agricultural production, and our daily life, leading to the globally deteriorated environment, especially in some developing countries [1,2]. In this condition, continuable development, species diversity, even the fundamental subsistence of animals and plants are threatened seriously. Fortunately, as the cognition on the significance of environment is being deepened in our mind, more and more efforts have been devoted to the detection and treatment of environmental contaminants [3–5].

Persistent organic pollutants (POPs), e.g., mirex, DDTs, and aldrin, are greatly noxious chemicals in environment remained from pesticides [6,7]. The usage of POPs has been strictly restricted by the "Stockholm convention on POPs", which was enacted on United Nations Conference in 2001. POPs can cumulate in organism among generations and transfer between different species [8,9]. Therefore, it is significant to detect POPs for both environmental evaluation and further treatment. In recent years, many approaches have been developed to detect POPs, such as gas chromatography [10], electrochemical methods [11,12], and surface-enhanced Raman scattering [13]. However, developing facile approach with simple operation, low-cost without the requirements of expensive equipments and high energy, and portable instruments for the detection of POPs still remains a great challenge.

Gas sensor, as a kind of important electronic device, has been widely applied in industry and daily life for real-time monitoring towards gas surroundings, such as ammonia and chlorine monitoring in chemical factory, methane detecting in coal mine, natural gas monitoring in kitchen, etc. Many conductive polymers and semiconductors have been developed as gas-sensing materials for the fabrication of gas sensors [14,15]. Among them, metal oxide semiconductors, e.g., SnO_2, ZnO, Cu_2O, and In_2O_3, are of particular interests due to their broad responding targets and rapid responses. However, the performance of such sensors is significantly influenced by the morphology and structure of sensing materials, resulting in a great obstacle for gas sensors based on bulk materials or thin films to achieve highly sensitive properties. It becomes a serious problem for further exploring novel applications of gas sensors. In the past few years, great achievements in the preparation of nanomaterials create new opportunities for developing highly sensitive gas sensors and further investigating their potential applications. Previously, we have reported some gas sensors based on nanoscale metal oxide semiconductors, which exhibited fascinating gas-sensing performance towards target gases, such as indoor air contaminants and other poisonous gases [16–18]. These findings

* Corresponding author. Tel.: +86 551 5591142; fax: +86 551 5592420.
E-mail address: jhliu@iim.ac.cn (J. Liu).

0039-9140/$ – see front matter © 2010 Elsevier B.V. All rights reserved.
doi:10.1016/j.talanta.2010.04.007

make it possible to develop novel approaches for the detection of POPs using nanomaterial-based gas sensors.

Herein, we report an innovative method for the detection of POPs using gas sensor. The presented approach, in which target POPs are distinguishable through recognizing characteristics in gas adsorption–desorption cycles, is facile without the requirements of complex operations, expensive and bulky instruments. Porous tri-walled SnO_2 nanostructures which were employed as gas-sensing materials in sensor to achieve a highly sensitive performance were characterized. Furthermore, the gas-sensing mechanism towards POPs was also demonstrated from the aspects of charge transfer and kinetic processes of gas adsorption and desorption.

2. Experimental

2.1. Preparation of porous tri-walled SnO_2 nanostructures

All chemicals were analytical grade and used without further purification as purchased from Shanghai Chemical Reagents Company. A hydrothermal route followed by annealing process, which was close to the previous reference [19], was employed for the preparation of SnO_2 nanostructures. In a typical procedure, 20 mmol fructose and $SnCl_4{\cdot}5H_2O$ were dissolved into deionized water to form a homogeneous solution (40 mL) by stirring and ultrasonication alternately. And then, the solution was transferred into a Teflon-lined stainless steel autoclave with a capacity of 50 mL. The autoclave was sealed and kept in an oven at a constant temperature of 170 °C for 12 h. Subsequently, the autoclave was taken out and allowed to cool to room temperature naturally. The brown precipitate was collected by centrifugation and washed with ethanol and deionized water for several times. After being dried, the as-obtained samples were further annealed in a furnace at 550 °C for 1 h in air.

2.2. Material characterization

Morphology and structure of the as-prepared products were characterized by a FEI Sirion 200 field-emission scanning electronic microscopy (FESEM), and a Hitachi H-800 transmission electron microscope (TEM) at an accelerating voltage of 200 kV. High-resolution TEM (HRTEM) images, selective area electron diffraction (SAED) pattern, and energy dispersive X-ray spectroscopy (EDX) spectrum were obtained on a JEOL-2010 transmission electron microscope equipped with an Oxford windowless Si (Li) detector. Surface state analysis was carried out on an ESCALab MK II X-ray photoelectron spectrometer (XPS) using non-monochromatized Mg Kα X-ray beams as excitation source. Binding energies in all XPS spectra were calibrated using that of C 1s (284.6 eV). Brunauer–Emmett–Teller (BET) surface area of the samples was measured on a Coulter Omnisorp 100CX instrument by using N_2 adsorption and desorption.

2.3. Fabrication of gas sensor

Structure of the as-fabricated gas sensor based on SnO_2 nanomaterials is shown in Fig. 1. There was a pair of comb-like gold electrodes fixed on the surface of Al_2O_3 ceramic substrate (5 mm × 2 mm × 0.5 mm) by screen-printing technique. A RuO_2 layer as heater connected by two gold electrodes at each end was also coated on the back side. The as-prepared SnO_2 nanomaterials were dispersed into a certain amount of ethanol under ultrasonication. And then, the formed suspension was coated onto the surface of Al_2O_3 ceramic substrate at the side with comb-like gold electrodes. Finally, it was dried and further welded to fabricate device for detection.

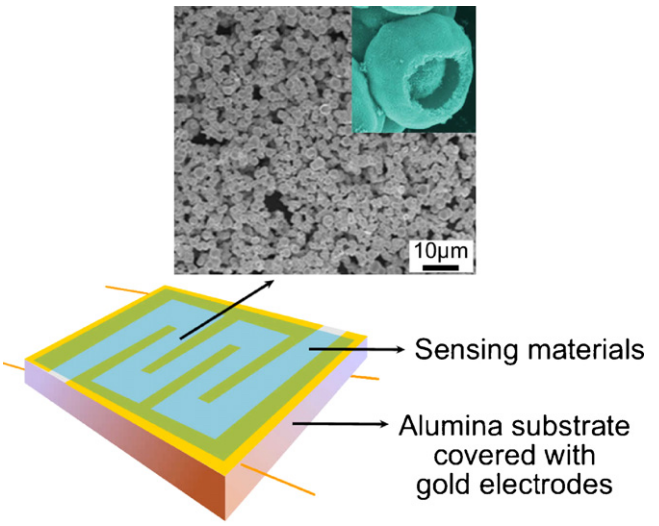

Fig. 1. Structure of the as-fabricated gas sensor based on porous tri-walled SnO_2 nanostructures.

2.4. Construction of gas sensor-based system for POPs detection

The gas sensor-based system for POPs detection was mainly constructed by three parts, i.e., gas carrier, gasification and detection chambers. In our study, methoxychlor, mirex, p,p′-DDT, and aldrin as typical organochlorine pesticides were employed as target POPs for detection. Methoxychlor and mirex were dissolved in hexane and benzene in a concentration of 1.0×10^{-4} g L^{-1}, respectively. Similarly, ligroine dissolved with p,p′-DDT or aldrin in a concentration of 1.0×10^{-3} g L^{-1} were also prepared. In gas-sensing detection, the injected volumes of each sample are 1, 2, and 5 μL, respectively. For comparison, pure hexane, benzene, and ligroine which served as solvents in POP solutions were also detected. In a typical operation, firstly, liquid sample was injected into gasification chamber to transform into vapor by heating at a temperature of 200 °C. It should be indicated that these compounds would not be decomposed in this condition due to their characteristic nature. Secondly, the as-formed vapor was transferred into detection chamber by constant air flow (15 sccm) which served as gas carrier. Once the target gas contacted with gas-sensing nanomaterials, responding signal (current) would be recorded by a computer-controlled gas-detecting system in which a Keithley-6487 picoameter/voltage sourcemeter was used as both current recorder and power source. At last, exhaust gases were collected by a solution at the end of the system.

The sensitivity (S) of gas sensor was defined as the following equation:

$$S = \frac{R_{air}}{R_{gas}} = \left(\frac{I_{gas}}{I_{air}}\right)_V \quad (1)$$

where R_{air} is the resistance in gas carrier (pure air) and R_{gas} is that in the gas mixture of gas carrier and targets (vapors of POPs and/or solvents). According to the Ohm's Law [20], in which current is inversely proportional to resistance under constant voltage, S can also be presented by the current in gas carrier (I_{air}) and in gas mixture (I_{gas}) mentioned above in the condition of constant measuring voltage.

3. Results and discussion

3.1. Characterizations of SnO_2 nanostructures

Typical morphology and structure of the as-prepared materials are shown in Fig. 2. As can be observed from FESEM images (Fig. 2a

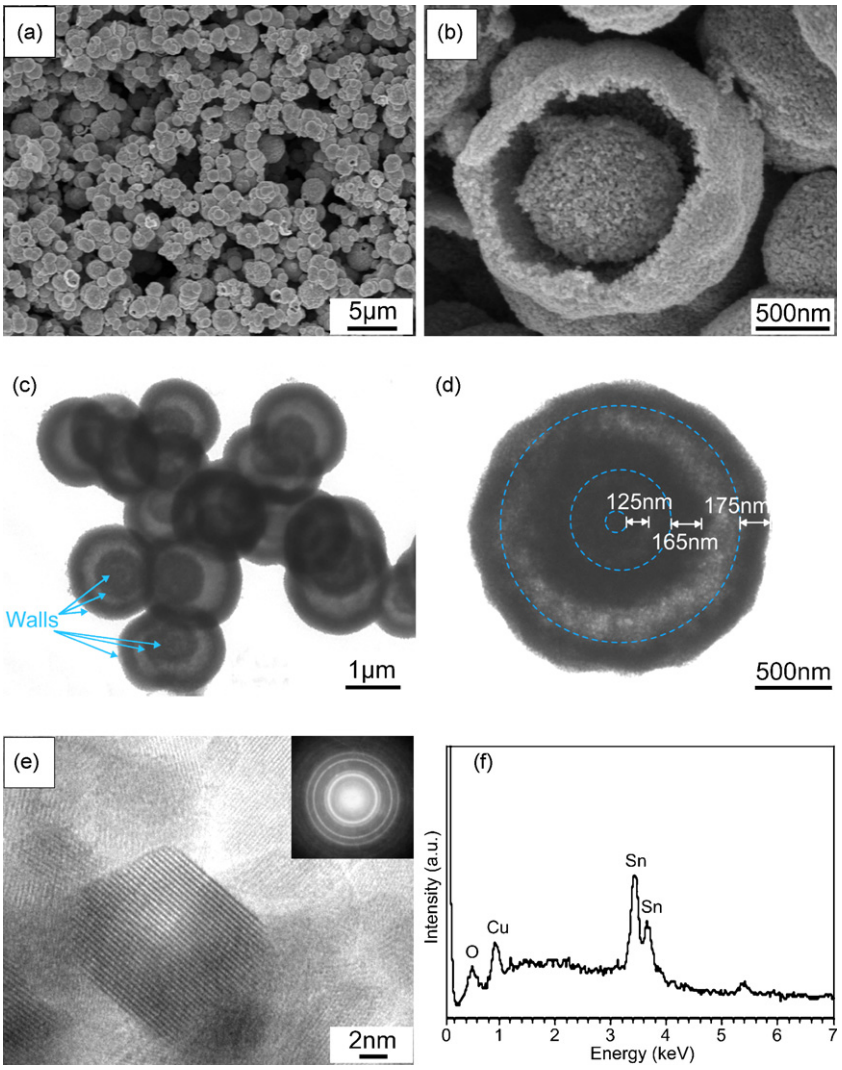

Fig. 2. (a) Low- and (b) high-magnification FESEM images, (c) TEM micrograph, (d) low-magnification and (e) lattice-resolved HRTEM images inserted with corresponding SAED pattern, and (f) EDX spectrum of the as-prepared materials.

and b), the products exhibit a special tri-walled spherical morphology with porous and hollow structures, which can be confirmed by TEM image (Fig. 2c). Each porous sphere, which is in a diameter of ca. 2 μm, is consisted of numerous congregated nanoparticles. Seen from HRTEM images (Fig. 2d), the thicknesses of external, middle, and internal walls are ca. 175, 165, and 125 nm, respectively. The profile of internal wall is not so obvious can be ascribed to the large thickness of multiple walls. In Fig. 2e, it can be observed that the particle-size ranges from 15 to 20 nm approximately. Besides, well-arranged crystalline lattice fringes in Fig. 2e combined with the inserted ring-like SAED pattern indicate a well-crystallized polycrystalline structure. EDX analysis (Fig. 2f) shows the presence of Sn and O elements without impurities (the appearance of copper signal results from the copper grid in measurement) in a molar ratio of ca. 1:1.986, which is in good agreement with the stoichiometry of SnO_2 compound.

The composition and surface state of as-obtained products were further investigated by XPS spectra, as shown in Fig. 3. Peaks of Sn, O, together with C, can be clearly observed in survey spectrum (Fig. 3a). The signal of C comes mainly from atmospheric contamination due to the exposure of samples to air [21,22]. From the survey spectrum, it is revealed that SnO_2 products are pretty pure, which is consistent with the result of EDX. In Fig. 3b, peaks located at ca. 487.1 and 495.6 eV can be assigned to Sn $3d_{5/2}$ and Sn $3d_{3/2}$ in SnO_2, respectively [23,24]. As to the XPS spectrum of O 1s (Fig. 3c), two shoulders can be observed in addition to the main peak at 530.7 eV which is assigned to the lattice oxygen in SnO_2 crystals [25]. The asymmetric O 1s peak was further fitted with three Gaussian functions for comparison. The peak centered at ca. 531.9 eV can be attributed to Sn–OH groups and chemisorbed oxygen species (O_2^-) [26,27], while the one at 533.4 eV is ascribed to adsorbed H_2O on the surface of products [28]. The existence of numerous functional groups and chemisorbed oxygen species indicates an active surface of the as-prepared SnO_2 nanostructures.

As surface area is another key factor for influencing gas-sensing performance in addition to the surface state of materials, surface area was also measured via a BET method (the N_2 adsorption–desorption isotherm was not shown here). A type-IV isotherm with a hysteresis loop ranging from 0.4 to 1.0 (P/P_0) was found, implying a mesoporous structure (pore-size ranges from 2 to 50 nm) [29] of the SnO_2 nanostructures which is in agreement with HRTEM observations. Through BET analysis, it is found that the surface area of SnO_2 samples is 36.5 $m^2\ g^{-1}$, indicating a strong adsorption ability towards gas molecules. Besides, it is revealed that the SnO_2 nanomaterials exhibit a narrow pore-size distribution centered at ca. 19.6 nm. By combining the large active surface

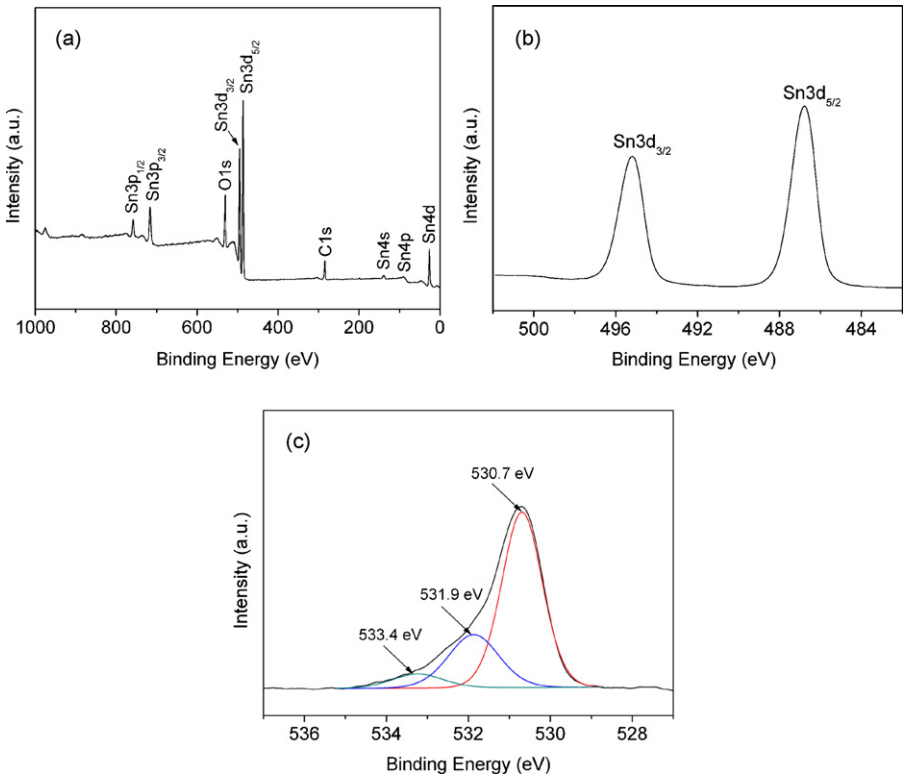

Fig. 3. XPS spectra of the as-prepared samples: (a) survey spectrum; (b) Sn 3d; and (c) O 1s spectra.

that is significant for surface contact reactions, with porous and hollow structures which are advantageous for gas adsorption and desorption, it is indicated that the as-prepared SnO_2 nanomaterials could be promisingly applied in gas sensors to achieve a highly sensitive performance.

3.2. Gas-sensing detection towards POPs and mechanism investigation

Fig. 4 shows the real-time responding curves of gas sensor based on porous tri-walled SnO_2 nanomaterials in gas detection.

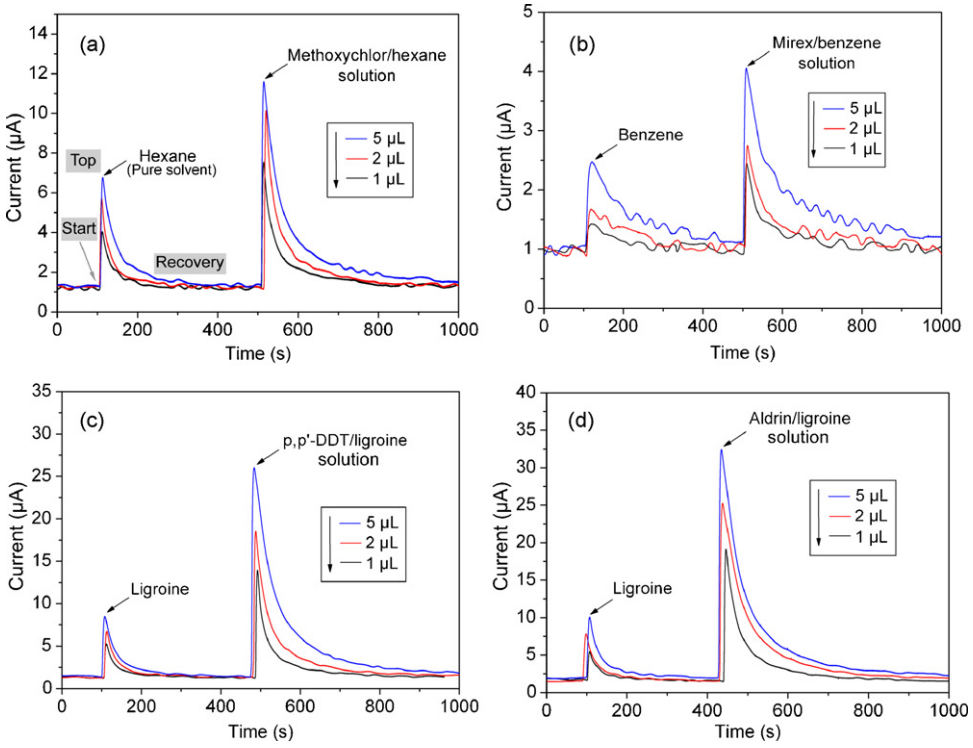

Fig. 4. Real-time responding curves of gas sensor towards different samples: (a) hexane (as solvent), and methoxychlor/hexane solution (1.0×10^{-4} g L^{-1}); (b) benzene, and mirex/benzene solution (1.0×10^{-4} g L^{-1}); (c) ligroin, and p,p′-DDT/ligroin solution (1.0×10^{-3} g L^{-1}); (d) ligroine, and aldrin/ligroine solution (1.0×10^{-3} g L^{-1}).

In all measurements, solvents were injected first, and then the POP/solvent mixtures were injected later. For the recovery of gas sensor which will be demonstrated below, air flow (with O_2) was employed as gas carrier rather than some traditional carriers, such as Ar and N_2. As can be seen in Fig. 4, current increases rapidly after injecting sample without the consideration of short time for gasification and vapors transferring, indicating that the resistance of gas sensor decreases while contacting with target gases according to Ohm's law. Besides, in Fig. 4, it is revealed that all sensitivities towards POPs solutions are remarkably higher than that of pure solvents. As compared with some conventional detecting methods, the presented approach is fast and facile with simple operation, low-cost without the requirements of large and expensive equipments (e.g., gas chromatography/mass spectrometry). The porous SnO_2 sensor-based route makes it promising to develop portable instruments for the detection of POPs.

In order to demonstrate the gas-sensing mechanism towards POPs, a tri-leveled variation of potential barrier in addition to a charge transfer process is proposed, as illustrated in Fig. 5. In air surroundings, O_2 is adsorbed on the surface of SnO_2 nanomaterials. And then, the adsorbed O_2 traps and reacts with electrons from SnO_2 to produce negative oxygen species, e.g., O_2^- and O^{2-} [30], which can be supported by XPS analysis presented above. As the achievement of equilibrium of such chemical reactions, a space charge layer which serves as a potential barrier for electron transfer is formed [31]. The electrical conductivity σ depends on barrier height ($q|V_B|$), as shown in Eq. (2) [32],

$$\sigma = e^{-(q|V_B|/kT)} \tag{2}$$

where q, V_B, k, and T are elementary electron charge, potential, Boltzmann's constant, and temperature, respectively. Besides, since barrier can be approximately expressed as Eq. (3),

$$q\left|V_B\right| \propto (N_t^-)^2 \tag{3}$$

where N_t^- can be modified by charge transfer during surface contact reactions with gas molecules, the conductivity can be impacted greatly by gas surroundings [33]. In our study, a tri-leveled barrier would be obtained due to the special structure of SnO_2 nanomaterials with three walls by considering each wall as a whole. It is indicated that the total potential barrier (E_{air}) would be remarkably enhanced by the integration of each barrier of walls, resulting in an enlarged resistance of SnO_2 nanostructure-based gas sensor in air.

By contraries, when gas sensor is exposed to vapors of POPs, which are reducing gases, reactions between negative oxygen species and vapors of POPs will occur. In this process, electrons are released [34], thereby reducing the thickness of space charge layer, and leading to the decrease of potential barrier (E_{POPs}). As a result, the high resistance of SnO_2-based gas sensor in air is decreased in vapors of POPs. Moreover, in our study, the particle-size (15–20 nm) of SnO_2 nanostructures belongs to the case of $D \geq 2L$ (D and L are particle-size and thickness of space charge layer, respectively) in Rothschild's model [35], in which potential barrier is controlled by the neck between particles. Therefore, current constriction effect combined with the effect of grain boundaries would also be potential explanations for the enhanced sensitivity.

As gas-sensing process is based on surface contact reactions, the kinetic process of gas adsorption–desorption is also significant for understanding gas-sensing mechanism. In our study, the gas-responding curve was further transformed for the investigation of gas adsorption–desorption process. Taking the gas detection towards 1 μL methoxychlor/hexane solution for example, gas-sensing response (I, i.e., current of gas sensor in our investigation) was transformed from y-axis to x-axis, while the first derivative

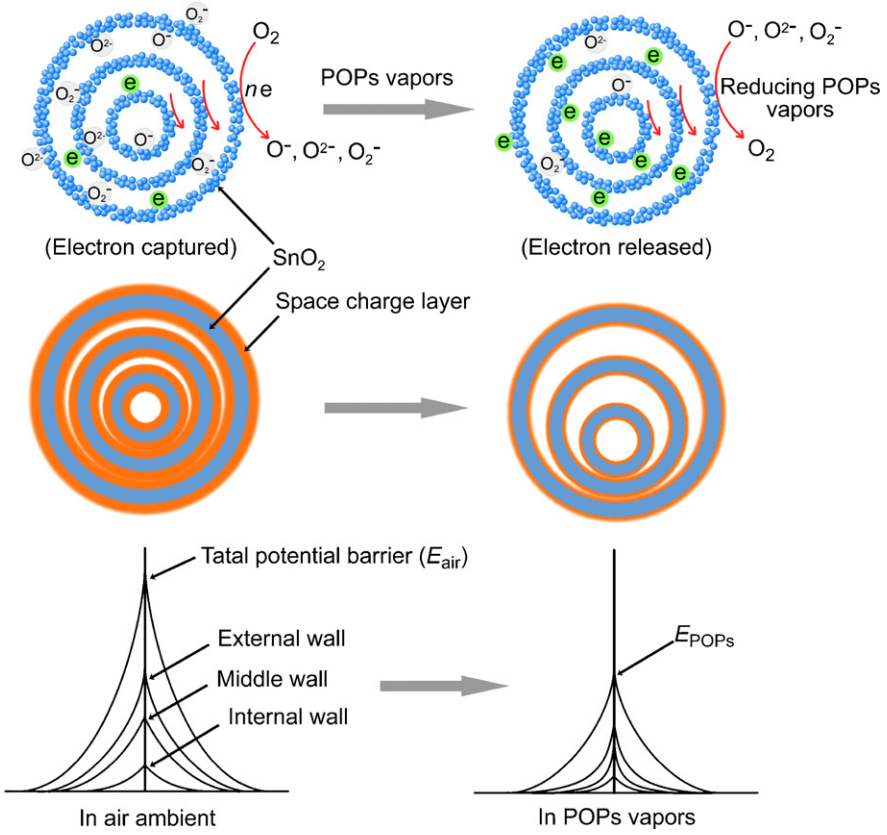

Fig. 5. Illustration of gas-sensing mechanism of porous tri-walled SnO_2 nanostructures towards vapors of POPs.

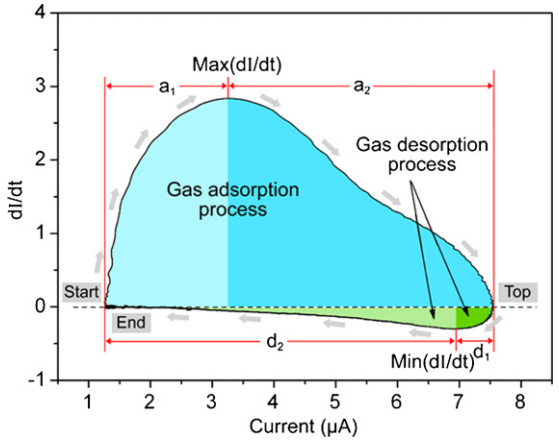

Fig. 6. Gas adsorption (above the dashed line)–desorption (below the dashed line) curve of gas sensor towards 1 μL methoxychlor/hexane solution.

of response towards time was set as *y*-axis, as shown in Fig. 6. In Fig. 6, it is labeled for the indication of gas adsorption–desorption process corresponding to Fig. 4a. Under a certain working condition, including temperature, surface state of gas-sensing materials, ambient gas composition, and measuring voltage, the resistance of gas sensor is fixed, in other words, the current is determined. Therefore, the current of gas sensor can effectively present the surface state of gas-sensing materials in a determined working condition, and hence reflecting the gas adsorption–desorption process in gas detection.

Seen from part a_1 in Fig. 6, gas-sensing response increases rapidly due to the adsorption of target gas for contact reactions in which numerous captured electrons are released. As reactions turn to be in equilibrium, and target gas passes through the gas sensor by gas carrier, the increase of response slows down gradually, as shown in part a_2. Accompanying with the gas adsorption process, the products of gas-sensing reactions are desorbed simultaneously. However, at the initial stage (part a_1 and a_2), gas adsorption plays a dominate role as compared with desorption. In contrast, at late period (part d_1 and d_2), gas desorption becomes overwhelming due to the replacement of adsorbed molecules by gas carrier, leading to the recovery of gas sensor back to initial state finally. As gas adsorption–desorption process is reflected by the transformed gas-responding curve, some characteristics from such curve, e.g., sensitivity (S), max(dI/dt), min(dI/dt), can be extracted for the recognition of target gases via feature extraction method followed by discriminant analysis [36], which is similar to electronic nose system with gas sensor array [37]. It is suggested that target POPs are potentially distinguishable via the presented gas sensor-based detecting method.

3.3. Preliminary study on distinguishable analysis

As one of the typical metal oxide semiconductors, SnO_2 has been demonstrated to respond to H_2 [38], CO [39], H_2S [40], ethanol [41], CH_4 [42], and NO_2 [43]. In our study, the porous SnO_2 sensor responded to both solvents and POPs with increasing current values in measurements, leading to a challenge for distinguishable analysis towards samples. Besides the traditional methods using sensitivity as distinguishable characteristic, we have investigated a new approach for potentially distinguishable analysis using characteristics extracted from the kinetic processes of gas adsorption–desorption. Fig. 7 shows the comparison on charac-

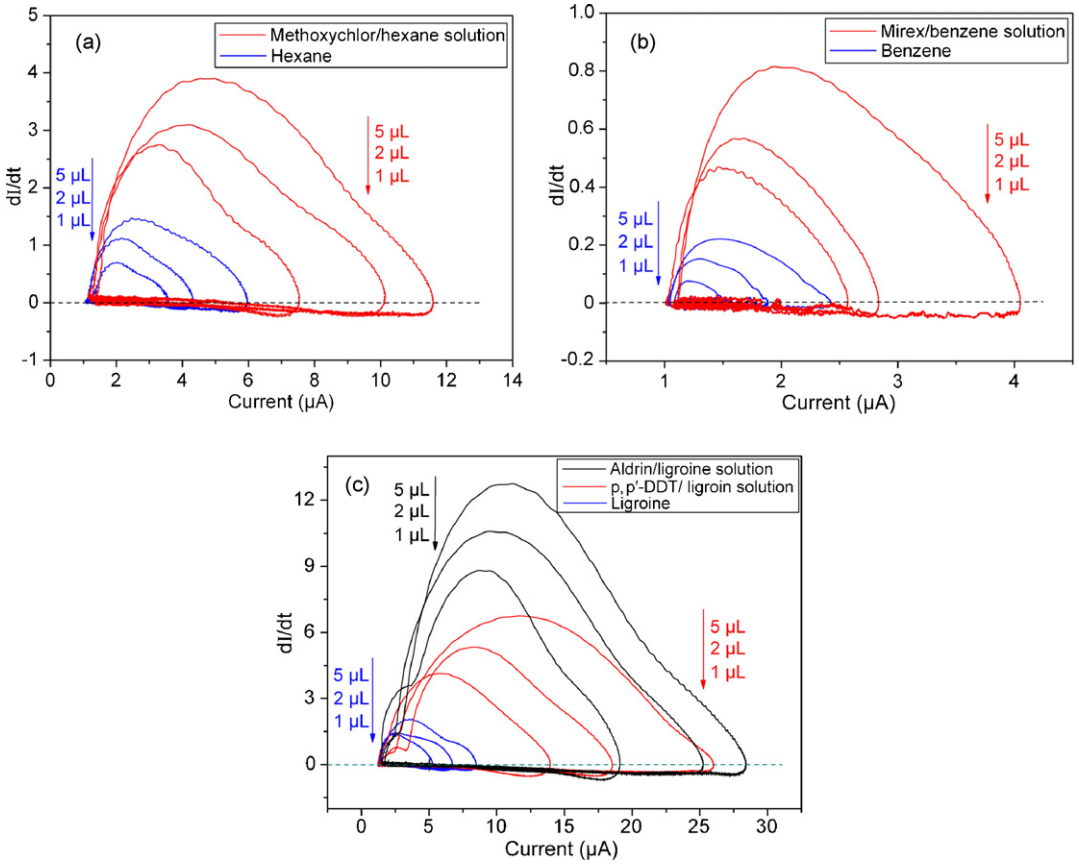

Fig. 7. Gas adsorption–desorption curves of gas sensor towards different samples: (a) hexane (pure solvent), and methoxychlor/hexane solution (1.0×10^{-4} g L^{-1}); (b) benzene, and mirex/benzene solution (1.0×10^{-4} g L^{-1}); (c) ligroin, p,p′-DDT/ligroin solution (1.0×10^{-3} g L^{-1}), and aldrin/ligroin solution (1.0×10^{-3} g L^{-1}).

Table 1
Typical characteristics in gas adsorption–desorption curves of gas sensor towards p,p′-DDT and aldrin solutions.

Sample volume (μL)	Sensitivity, S		max(dI/dt)		min(dI/dt)	
	p,p′-DDT solution	Aldrin solution	p,p′-DDT solution	Aldrin solution	p,p′-DDT solution	Aldrin solution
1	11.7	15.8	4.1	7.3	−3.6	−5.1
2	15.4	21.1	5.4	10.5	−3.7	−5.1
5	21.6	23.8	6.8	12.6	−3.6	−5.2

teristics in gas adsorption–desorption processes towards different samples. As can be seen, gas adsorption–desorption curves of POPs solutions are remarkably different from that of pure solvents. It is indicated that POPs solutions are distinguishable from pure solvents due to the significant variation of characteristics in curves, including sensitivity, max(dI/dt), and min(dI/dt). In addition to the different values extracted from gas adsorption–desorption curves, the shapes of curves are also variant with each other. The good structural symmetry is not advantage for adsorption–desorption and surface contact reactions, leading to a mild change of curve shapes, such as benzene (Fig. 7b). As for other samples, the structural polarity would turn the curve shapes to be more acute, especially during gas adsorption processes, as shown in Fig. 7a. Moreover, the size of molecules would also be a potential factor for influencing gas adsorption–desorption processes. At the same concentration, gas adsorption–desorption processes of gas sensor towards POPs solutions are also different with each other, like mirex versus methoxychlor, and p,p′-DDT versus aldrin, suggesting that target POPs are also potentially recognizable. For comparison, gas adsorption–desorption curves of p,p′-DDT and aldrin solutions with the same solvent at a determined concentration are presented in Fig. 7c. Besides to the difference of curves between POPs solutions and pure solvent, the characteristics in gas adsorption–desorption processes towards p,p′-DDT and aldrin solutions are also different as mentioned above. It indicates that the selectivity issue of some traditional SnO_2 sensors could be potentially overcome by kinetic analysis of gas adsorption–desorption, and thereby enables the presented approach to distinguish different samples effectively.

Typical characteristics obtained from Fig. 7c, including sensitivity, max(dI/dt), and min(dI/dt), were listed in Table 1 for further demonstration. It can be found that it is difficult to distinguish each sample only by comparing the sensitivities of gas sensor towards p,p′-DDT and aldrin solutions because of the interlacement of values. For example, the sensitivity of gas sensor towards 5 μL p,p′-DDT solution (S = 21.6) is close to that for 2 μL aldrin solution (S = 21.1). However, by combining the values of sensitivity, max(dI/dt), and min(dI/dt), POPs solutions can be feasibly distinguished with each other. In other words, even with a similar sensitivity, the distinguishability of target POPs are also achievable by means of comparing values of max(dI/dt) and min(dI/dt) in kinetic curves of gas adsorption–desorption simultaneously. It would be also feasible for the comparison of POPs solutions at different concentrations with the same injected volume, which is on the way of our further exploration. As for the sample of 5 μL p,p′-DDT solution with a similar sensitivity to 2 μL aldrin solution mentioned above, the values of max(dI/dt) and min(dI/dt) (6.8 and −3.6, respectively) are remarkably different with that of 2 μL aldrin solution (10.5 and −5.1, respectively), indicating a significant distinguishability between them by the additional analysis towards typical characteristics in kinetic process of gas adsorption–desorption.

4. Conclusions

In summary, a facile gas sensor-based approach for the detection of POPs was developed for the first time. To achieve a highly sensitive performance, porous SnO_2 nanostructures with a special tri-walled structure were employed as gas-sensing materials in sensor. Gas-sensing mechanism towards POPs is demonstrated from two aspects, i.e., charge transfer and kinetic processes of gas adsorption and desorption. Through gas detection, it is revealed that the gas responses and adsorption–desorption processes towards target POPs, including mirex, methoxychlor, p,p′-DDT, and aldrin, are remarkably different from that of pure solvents, and even significantly different among themselves. By comparing characteristics in gas adsorption–desorption curves, each POP can be distinguished. As the developed innovative approach, which is facile without the demands of complex operations, expensive and bulky instruments, provides new opportunities for the detection of POPs, it is expected that it could be potentially applied for environmental monitoring.

Acknowledgments

This work was financially supported by the State Key Project of Fundamental Research for Nanoscience and Nanotechnology (Grant No. 2007CB936603), and the National Natural Science Foundation of China (Grant Nos. 10635070, 60604022 and 60574094). Moreover, Prof. Maosheng Ma from University of Science and Technology of China was appreciated for the helpful analysis and discussion on XPS spectra.

References

[1] R.A. Hites, J.A. Foran, D.O. Carpenter, M.C. Hamilton, B.A. Knuth, S.J. Schwager, Science 303 (2004) 226–229.
[2] M.L. Polizzotto, B.D. Kocar, S.G. Benner, M. Sampson, S. Fendorf, Nature 454 (2008) 505–509.
[3] R. Budd, A. O'Geen, K.S. Goh, S. Bondarenko, J. Gan, Environ. Sci. Technol. 43 (2009) 2925–2930.
[4] A.P. Esser-Kahn, A.T. Iavarone, M.B. Francis, J. Am. Chem. Soc. 130 (2008) 15820–15822.
[5] C.J. DiBlasi, H. Li, A.P. Davis, U. Ghosh, Environ. Sci. Technol. 43 (2009) 494–502.
[6] J.M. Blais, D.W. Schindler, D.C.G. Muir, L.E. Kimpe, D.B. Donald, B. Rosenberg, Nature 395 (1998) 585–588.
[7] Y. Yao, T. Harner, P. Blanchard, L. Tuduri, D. Waite, L. Poissant, C. Murphy, W. Belzer, F. Aulagnier, E. Sverko, Environ. Sci. Technol. 42 (2008) 5931–5937.
[8] B. Jimenez, R. Merino, E. Abad, J. Rivera, K. Olie, Environ. Sci. Pollut. Res. 14 (2007) 61–68.
[9] A.J. Hall, G.O. Thomas, A.J. McConneell, Environ. Sci. Technol. 43 (2009) 6364–6369.
[10] S.P.J. van-Leeuwen, J. Boer, J. Chromatogr. A 1186 (2008) 161–182.
[11] L. Tang, G.M. Zeng, G.L. Shen, Y.P. Li, Y. Zhang, D.L. Huang, Environ. Sci. Technol. 42 (2008) 1207–1212.
[12] S. Rubio, D. Perez-Bendito, Anal. Chem. 81 (2009) 4601–4622.
[13] L. Guerrini, A.E. Aliaga, J. Carcamo, J.S. Gomez-Jeria, S. Sanchez-Cortes, M.M. Campos-Vallette, J.V. Garcia-Ramos, Anal. Chim. Acta 624 (2008) 286–293.
[14] B. Li, G. Sauve, M.C. Iovu, M. Jeffries-EL, R. Zhang, J. Cooper, S. Santhanam, L. Schultz, J.C. Revelli, A.G. Kusne, T. Kowalewski, J.L. Snyder, L.E. Weiss, G.K. Fedder, R.D. McCullough, D.N. Lambeth, Nano Lett. 6 (2006) 1598–1602.
[15] A.F. Chen, S.L. Bai, B.J. Shi, Z.Y. Liu, D.Q. Li, C.C. Liu, Sens. Actuators B 135 (2008) 7–12.
[16] J.Y. Liu, Z. Guo, F.L. Meng, Y. Jia, T. Luo, M.Q. Li, J.H. Liu, Cryst. Growth Des. 9 (2009) 1716–1722.
[17] J.Y. Liu, Z. Guo, F.L. Meng, T. Luo, M.Q. Li, J.H. Liu, Nanotechnology 20 (2009) 125501.
[18] Z. Guo, J.Y. Liu, Y. Jia, X. Chen, F.L. Meng, M.Q. Li, J.H. Liu, Nanotechnology 19 (2008) 345704.
[19] H.X. Yang, J.F. Qian, Z.X. Chen, X.P. Ai, Y.L. Cao, J. Phys. Chem. C 111 (2007) 14067–14071.
[20] T. Isoda, H. Makimoto, H. Imanaga, R. Imamura, J. Pawlat, T. Ueda, Sens. Actuators B 123 (2007) 805–810.

[21] Q.L. Huang, M. Wang, H.X. Zhong, X.T. Chen, Z.L. Xue, X.Z. You, Cryst. Growth Des. 8 (2008) 1412–1417.
[22] S.Y. Cheng, Y.J. He, G.N. Chen, E.C. Cho, G. Conibeer, Surf. Coat. Technol. 202 (2008) 6070–6074.
[23] A.C. Deshpande, P.M. Koinkar, S.S. Ashtaputre, M.A. More, S.W. Gosavi, P.D. Godbole, D.S. Joag, S.K. Kulkarni, Thin Solid Films 515 (2006) 1450–1454.
[24] H.J. Ahn, H.C. Choi, K.W. Park, S.B. Kim, Y.E. Sun, J. Phys. Chem. B 108 (2004) 9815–9820.
[25] Q.R. Zhao, Z.G. Zhang, T. Dong, Y. Xie, J. Phys. Chem. B 110 (2006) 15152–15156.
[26] S. Kaciulis, G. Mattogno, A. Galdikas, A. Mironas, A. Setkus, J. Vac. Sci. Technol. A 14 (1996) 3164–3168.
[27] T. Moon, S.T. Hwang, D.R. Jung, D. Son, C. Kim, J. Kim, M. Kang, B. Park, J. Phys. Chem. C 111 (2007) 4164–4167.
[28] J.T. Kloprogge, L.V. Duong, B.J. Wood, R.L. Frost, J. Colloid Interface Sci. 296 (2006) 572–576.
[29] J.L. Mohanan, I.U. Arachchige, S.L. Brock, Science 307 (2005) 397–400.
[30] X.J. Huang, F.L. Meng, Z.X. Pi, W.H. Xu, J.H. Liu, Sens. Actuators B 99 (2004) 444–450.
[31] C.N. Xu, J. Tamakijki, N. Miura, N. Yamazoe, Sens. Actuators B 3 (1991) 147–153.
[32] G. Martinelli, M.C. Carotta, Sens. Actuators B 23 (1995) 157–163.
[33] N. Barsan, U. Weimar, J. Electroceram. 7 (2001) 143–150.
[34] R.S. Niranjan, Y.K. Hwang, D.K. Kim, S.H. Jhung, J.S. Chang, L.S. Mulla, Mater. Chem. Phys. 92 (2005) 384–389.
[35] A. Rothschild, Y. Komem, J. Appl. Phys. 95 (2004) 6374–6380.
[36] S.P. Zhang, C.S. Xie, M.L. Hu, H.Y. Li, Z.K. Bai, D.W. Zeng, Sens. Actuators B 132 (2008) 81–89.
[37] D. Ballabio, M.S. Cosio, S. Mannino, R. Todeschini, Anal. Chim. Acta 578 (2006) 170–177.
[38] G. Korotcenkova, B.K. Cho, L. Gulinac, V. Tolstoy, Sens. Actuators B 141 (2009) 610–616.
[39] H. Keskinen, A. Tricoli, M. Marjamaki, J.M. Makela, S.E. Pratsinis, J. Appl. Phys. 106 (2009) 084316.
[40] X.Y. Xue, L.L. Xing, Y.J. Chen, S.L. Shi, Y.G. Wang, T.H. Wang, J. Phys. Chem. C 112 (2008) 12157–12160.
[41] F. Song, H.L. Su, J. Han, D. Zhang, Z.X. Chen, Nanotechnology 20 (2009) 495502.
[42] A. Kok, A. Tischner, T. Maier, M. Kast, C. Edtmaier, C. Gspan, G. Kothleitner, Sens. Actuators B 138 (2009) 160–167.
[43] M. Epifani, J.D. Prades, E. Comini, E. Pellicer, M. Avella, P. Siciliano, G. Faglia, A. Cirera, R. Scotti, F. Morazzoni, J.R. Morante, J. Phys. Chem. C 112 (2008) 19540–19546.